Journal of Power Sources 215 (2012) 89–98

Contents lists available at SciVerse ScienceDirect

Journal of Power Sources

journal homepage: www.elsevier.com/locate/jpowsour

An integrated system combining chemical looping hydrogen generation process and solid oxide fuel cell/gas turbine cycle for power production with CO_2 capture

Shiyi Chen, Zhipeng Xue, Dong Wang, Wenguo Xiang*

Key Laboratory of Energy Thermal Conversion and Control of Ministry of Education, School of Energy and Environment, Southeast University, Nanjing 210096, China

HIGHLIGHTS

- ► CLHG process produces hydrogen with inherent CO_2 separation.
- ► SOFC/GT cycle is integrated with coal gasification and CLHG process.
- ► The plant has an electrical efficiency ~43% (LHV) and zero-CO_2-emission.
- ► Parameters such as SOFC temperature influence the plant performance.

ARTICLE INFO

Article history:
Received 24 February 2012
Received in revised form
24 April 2012
Accepted 26 April 2012
Available online 8 May 2012

Keywords:
Coal gasification
Chemical looping hydrogen generation
Solid oxide fuel cell
Gas turbine combined cycle
Carbon capture

ABSTRACT

In this paper, the solid oxide fuel cell/gas turbine (SOFC/GT) cycle is integrated with coal gasification and chemical looping hydrogen generation (CLHG) for electric power production with CO_2 capture. The CLHG-SOFC/GT plant is configurated and the schematic process is modeled using Aspen Plus® software. Syngas, produced by coal gasification, is converted to hydrogen with CO_2 separation through a three-reactors CLHG process. Hydrogen is then fueled to SOFC for power generation. The unreacted hydrogen from SOFC burns in a combustor and drives gas turbine. The heat of the gas turbine exhaust stream is recovered in HRSG for steam bottoming cycle. At a system pressure of 20 bar and a cell temperature of 900 °C, the CLHG-SOFC/GT plant has a net power efficiency of 43.53% with no CO_2 emissions. The hybrid power plant performance is attractive because of high energy conversion efficiency and zero-CO_2-emission. Key parameters that influence the system performance are also discussed, including system operating pressure, cell temperature, fuel utilization factor, steam reactor temperature, CO_2 expander exhaust pressure and inlet gas preheating.

1. Introduction

The combustion of fossil fuels such as coal for power generation is a major contributor of CO_2 emission into the atmosphere. It is widely accepted that CO_2 is a greenhouse gas which leads to climate change in recent years [1]. It is necessary to mitigate CO_2 emission imminently. Emerging renewable energies such as solar, wind and tidal energy are alternative candidates to substitute carbonaceous fossil fuels in the future, but at present they are not sufficient to cover the drastic increase in energy demand by the world [2]. Thus, the power generation through fossil fuel combustion remains to occupy a large portion of power generation in the world. CO_2 capture and storage (CCS) is an option to reduce greenhouse gas emissions for centralized plants. However, the currently available CO_2 capture techniques impose high energy penalties, around 8–12% [3]. It is necessary to develop potential technologies for power generation using fossil fuels with a high energy efficiency and low CO_2 emission.

Chemical looping combustion (CLC) is a novel process for heat and power generation with inherent separation of CO_2 [4–6]. An oxygen carrier is used to transport oxygen from air to the fuel. Metal oxide particles such as hematite Fe_2O_3 [7,8], nickel oxide NiO [9,10] and copper oxide CuO [11,12] are suitable oxygen carriers. A CLC system includes two reactors: a fuel reactor and an air reactor. In the fuel reactor, the oxygen carrier is reduced by the fuel, the gas product is CO_2 and steam vapor. In the air reactor, the reduced oxygen carrier is regenerated by air. The net reaction of CLC is the fuel combustion in the air, but with inherent separation of CO_2. CLC can be used for hydrogen generation [13–16]. Chemical looping hydrogen generation (CLHG) is derived from CLC for hydrogen

* Corresponding author. Tel.: +86 25 8379 5545; fax: +86 25 8771 4489.
E-mail address: wgxiang@seu.edu.cn (W. Xiang).

0378-7753/$ – see front matter
doi:10.1016/j.jpowsour.2012.04.087

production with inherent separation of CO_2 [17–19]. Oxygen carriers used in CLHG are iron oxides [20–24], and the hydrogen production is via the traditional steam-iron process [25–27]. CLHG is mainly comprised of three reactors: a fuel reactor, a steam reactor and an air reactor, as shown in Fig. 1.

In the fuel reactor, the oxygen-rich hematite Fe_2O_3 is mostly reduced to wüstite $Fe_{0.947}O$ by the fuel gases:

$$1.803Fe_2O_3 + 1.601CO \rightarrow 1.601CO_2 + 3.807Fe_{0.947}O$$
$$\Delta H_{298} = 21.64\,\text{kJ mol}^{-1} \quad (1)$$

$$1.803Fe_2O_3 + 1.601H_2 \rightarrow 1.601H_2O + 3.807Fe_{0.947}O$$
$$\Delta H_{298} = 86.48\,\text{kJ mol}^{-1} \quad (2)$$

The gaseous outlet stream is composed of steam and CO_2. After water condensation, pure CO_2 is obtained. In the steam reactor, $Fe_{0.947}O$ reacts with steam. The solid product is magnetite Fe_3O_4 and the gas product is hydrogen:

$$3.807Fe_{0.947}O + H_2O \rightarrow 1.202Fe_3O_4 + H_2$$
$$\Delta H_{298} = -88.1\ \text{kJ mol}^{-1} \quad (3)$$

In the air reactor, magnetite is reoxidized to its original form hematite Fe_2O_3 by oxygen in the air. The reaction in the air reactor is strongly exothermic, which sustains the thermal balance of the three reactors:

$$4Fe_3O_4 + O_2 + 3.762N_2 \rightarrow 6Fe_2O_3 + 3.762N_2$$
$$\Delta H_{298} = -479.5\ \text{kJ mol}^{-1} \quad (4)$$

The net reaction of CLHG is the water–gas shift reaction, but with the advantage of inherent separation of hydrogen from CO_2.

$$CO + H_2O \rightarrow H_2 + CO_2 \quad \Delta H_{298} = -41.20\ \text{kJ mol}^{-1} \quad (5)$$

The solid oxide fuel cell (SOFC) is considered as a suitable candidate for electrical power plant application. SOFC has a high fuel cell efficiency with a high operating temperature, between 700 and 1000 °C. SOFC can be designed to operate at elevated pressure, which enables the integration with conventional gas turbine cycle. The combination of SOFC with gas turbine is regarded as one of the most promising power generating applications [28].

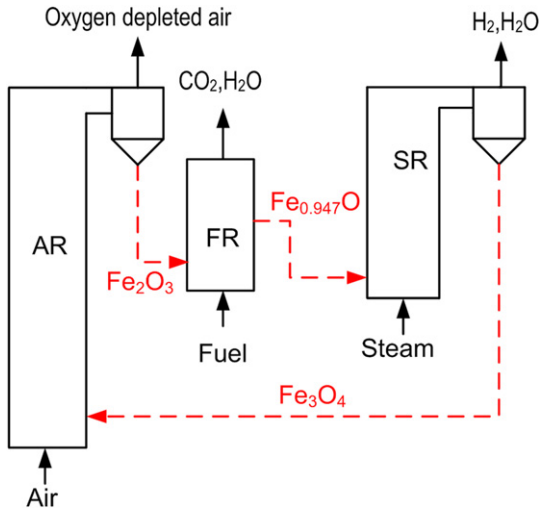

Fig. 1. The scheme of chemical looping hydrogen generation (CLHG) process.

There are extensive studies on the hybrid system of SOFC and gas turbine. Natural gas is usually used as the fuel in the hybrid SOFC-GT cycle. This is mainly because SOFC is operated at high temperature (around 700–1000 °C) under atmosphere or elevated pressures [29]. Under this condition, natural gas can be internally reformed to hydrogen and CO, which are reactants in the electrochemical reactions. Kim et al. [30–34] carried out a series of investigations on SOFC-GT hybrid systems. In their studies, atmosphere/pressured design [30], temperature constraints [31], fixed gas turbine design [32] are taken into consideration. Yi et al. [35] performed a sensitivity analysis of several major system parameters to identify the key development needs and design and operating improvements for the hybrid cycle. In their study, a system electrical efficiency higher than 75% could be achieved when the system operates under a high operating pressure (50 bar) and with a low percent excess air in SOFC. Granovskii [36] compared two combined SOFC/GT system. The difference was in the steam sources for gas reforming. One was with steam generation in the gas turbine cycle; the other was with a recycle of the exhaust gases around anodes of the SOFC stack. The results indicated at a fixed SOFC stack the scheme with recycling had better energy efficiency.

Besides used in large-scale centralized plants, the hybrid SOFC/GT system is also suitable for the small-scale power generating application in the distributed generation system of remote areas [37]. Uechi et al. [38] integrated a micro gas turbine and an SOFC, and it was confirmed that the hybrid system was greatly superior to a recuperated gas turbine in terms of power efficiency and aptitude for small-distributed generation. A 30-kW μGT-SOFC was shown to give power efficiency over 65% (LHV). Campanari [39] conducted the parametric analysis of small-scale recuperated SOFC/gas turbine cycles, and the projected electrical efficiency could exceed 65%.

With concerns of CO_2 mitigation, CCS is also implemented to the SOFC/GT hybrid system by many researchers [32,34,40–42]. Möller et al. [43] used genetic algorithm to optimize the SOFC/GT system with CO_2 capture. The SOFC/GT system could achieve an electrical efficiency above 60% with part capture of CO_2. Adams II et al. [44] investigated an electricity generation process using natural gas and SOFC. The process contained a steam reformer heat-integrated with cells to provide the heat necessary for reforming, and the cells were powered with hydrogen. The electrical efficiency was achieved as high as 74% HHV with 100% CO_2 capture. Kuramochi et al. [45] made an analysis of the competitiveness of CO_2 capture from an industrial solid oxide fuel cell combined heat and power system. Technical results showed that despite the energy penalties due to CO_2 capture and compression, net electrical and heat efficiencies were nearly identical with or without CO_2 capture because of higher heat recovery efficiency by separating SOFC off-gas streams for CO_2 capture.

Generally, using natural gas as fuel, the hybrid SOFC-GT efficiency could achieve an electrical efficiency above 60% [35–39,44,46,47], however, coal is the most abundant fossil fuels in the world. It has a wide geological distribution and low prices in the market compared with natural gas [48]. Gasification, along with new cleanup and sequestration technologies, allows an environmentally advantageous use of coal for power generation [49,50]. The gasification product from the coal is syngas. After gas cleaning, the syngas can be directly fueled in the SOFC stacks [28,51,52].

Liese [53] examined four arrangements of SOFC within a coal gasification cycle, it was found that the integrated gasification fuel cell cycle demonstrated significant efficiency advantages compared with IGCC with CO_2 capture, and the hydrogen fueled cell system had better net electricity compared with post-anode

CO_2 capture cases. Barton et al. [54] proposed a high-efficiency power production process from coal gasification with carbon capture. In their configuration, syngas from gasifier was shifted to hydrogen before anode, which enabled the recovery of CO_2 with a very small energy penalty and offered a high overall thermal efficiency.

Like most fuel cells, SOFC operates better on hydrogen than conventional fuels [50]. Compared to syngas or natural gas, there are several benefits using hydrogen as fuel in SOFC:

(i) Hydrogen has a better kinetics in electrochemical reactions. It should be noted that the reaction rate of CO electro-oxidation is much slower than that of hydrogen electro-oxidation [29,55]. Only a little CO is directly oxidized in the anode. Most of the methane or CO is converted to hydrogen through the reforming and the shift reactions before electrochemical oxidation [46].
(ii) Using hydrogen as fuel in SOFC, carbon deposition on the cell stack is completely avoided.
(iii) The possible mismatching of exothermic electrochemical reactions and the endothermic reforming may cause the temperature gradient along the electrode, resulting in the formation of local "hot" or "cold" spots [29] and causing severe thermal stress of the cell material [31]. The use of hydrogen as fuel gas provides a unique exothermic environment, and may offer a better temperature distribution inside the cell.
(iv) In the point of view of CO_2 capture, CO_2 can be sequestrated and captured in the hydrogen generation process before SOFC. Compared with post-combustion capture, the pre-combustion capture is predicted to reduce energy penalties because of a smaller gas flow volume processed and higher partial CO_2 pressure [41,56].

CLHG can be also combined with gas turbine cycle [57–61]. In this paper, SOFC/GT is integrated with coal gasification and CLHG for power generation with CO_2 capture. Syngas from gasifier is converted to hydrogen with CO_2 separation through the CLHG process. Hydrogen is then used to power SOFC/GT cycle. The main purpose is to investigate the thermodynamic performance of the coal fueled CLHG-SOFC/GT hybrid plant, and sensitivity analysis is also conducted.

2. Plant configuration and modeling

The layout of the CLHG-SOFC/GT hybrid plant integrated with coal gasification is shown in Fig. 2. The plant is comprised of six parts: gasification block, CLHG process, SOFC, gas turbine cycle, steam bottoming cycle and CO_2 compression. Coal is gasified in the gasifier. The hot raw syngas is quenched to 900 °C by recycling a portion of resulting syngas, and then is cooled to 350 °C in the waste boiler for gas cleaning. The heat recovered in the waste boiler is used to superheat and reheat the steam from the high pressure steam turbine. After gas cleaning, the syngas is used as the fuel gas of the chemical looping hydrogen generation process. Steam bled from the steam turbine is injected into the steam reactor. The hydrogen from the steam reactor is fed to the anode, and the oxygen depleted air from the air reactor is led to the cathode. The anode exhaust stream contains unreacted hydrogen, which is burnt in the combustor with the exhaust air from the cathode. The flue stream from the combustor is led to the gas turbine for power generation and the waste heat is recovered in the air HRSG for steam bottoming cycle. CO_2 stream from the fuel reactor expands in the CO_2 expander and cooled in CO_2 HRSG, providing additional heat to the steam bottoming cycle for an efficient energy recovery. CO_2 is then compressed and cooled in series of inter-cooling compressors to a pressure for pipeline.

2.1. Gasification block

Illinois 6# bituminous coal is selected in this work. The coal analysis is shown in Table 1. In the gasifier, coal is converted to syngas, an admixture of CO, H_2, H_2O, CO_2 and other gaseous impurities. The commercially available Shell gasification process is selected in this study. Compared with the wet slurry-fed gasification technology, the dry fed gasifier has higher cold gas efficiency [62,63]. Air separation unit (ASU) is not modeled here because the plant is already a complex system, but the specific work is adopted, 0.325 kW h kg^{-1} O_2 [64]. The gas compositions from the ASU are 95 vol.% O_2 with 4 vol.% Ar and 1 vol.% N_2. The coal powder is blown

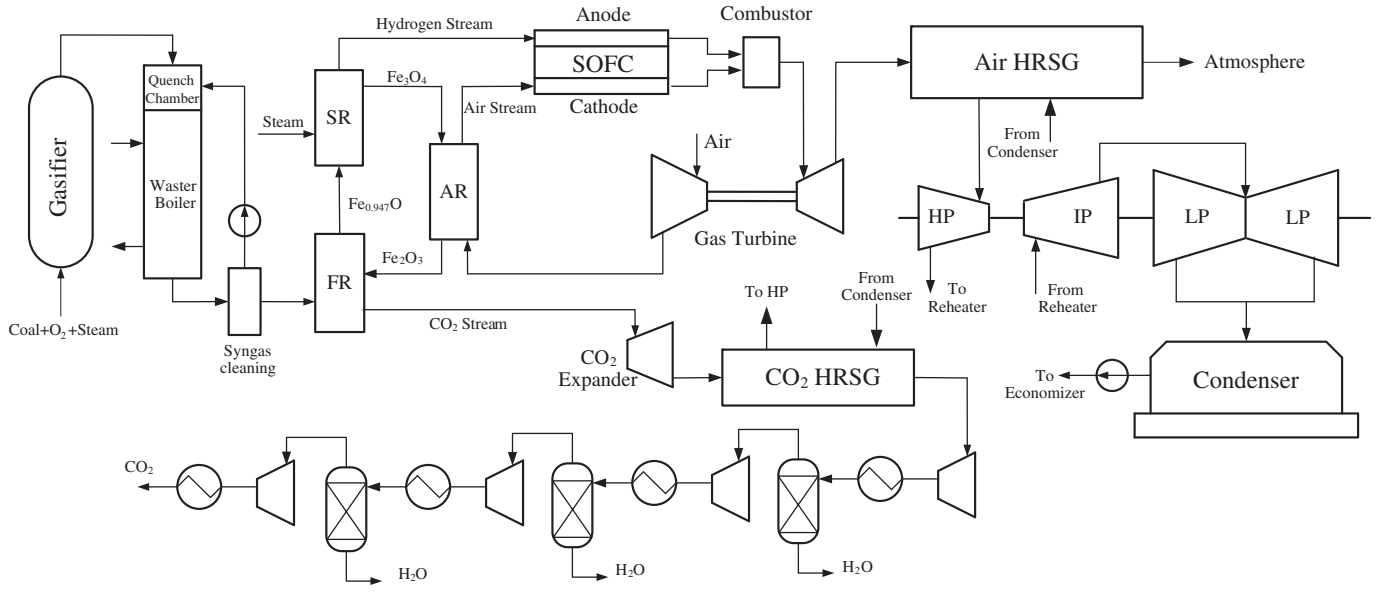

Fig. 2. Schematic layout of the CLHG-SOFC/GT hybrid plant integrated with coal gasification.

Table 1
Analysis of Illinois 6# bituminous coal.

Proximate analysis/% (mass, air dry)		Ultimate analysis/% (mass, air dry)	
Moisture	5.0	C	66.07
Volatile	39.24	H	5.07
Fixed carbon	46.26	O	9.5
Ash	9.5	N	1.19
		S	3.67
Lower heating value (LHV)/MJ kg^{-1}		26.805	

to the gasifier using CO_2 instead of nitrogen because nitrogen would end up as an impurity in the CO_2 stream. The detailed gasification conditions are summarized in Table 2.

2.2. Chemical looping hydrogen generation

As mentioned above, the CLHG process includes three reactor vessels: a fuel reactor, a steam reactor and an air reactor. The solid oxygen carrier circulating among the three reactors is iron oxide. In the fuel reactor, the cleaned syngas reacts with hematite Fe_2O_3, the gas product is CO_2 and steam vapor. The solid products are a mixture of wüstite FeO and magnetite Fe_3O_4. The reduced wüstite FeO and magnetite Fe_3O_4 enters the steam reactor and is oxidized to magnetite Fe_3O_4 by steam vapor, generating hydrogen. Magnetite Fe_3O_4 from the steam reactor is led to the air reactor and regenerated to hematite Fe_2O_3 by air. To get a full conversion of syngas, a compact fuel reactor is adopted. The detailed configuration could refer to the former work [19,57]. In order to improve the reactivity against agglomeration or sintering, hematite Fe_2O_3 is supported with inert material $FeAl_2O_4$.

2.3. Solid oxide fuel cell

Solid oxide fuel cell (SOFC) is a device which enables a conversion of chemical energy directly to electricity from fuel gas via electrochemical reactions rather than combustion. The high irreversibility within the combustor leads to drastic losses in the thermal efficiency [46]. Therefore, without the thermodynamic Carnot limitation, SOFC has a higher electrical efficiency than a conventional heat engine [65]. The electrical efficiency is usually between 40 and 60% [30]. Taking hydrogen as fuel, in an SOFC, the electric power is generated through the following process:

$$\text{Anode}: \quad H_2 + O^{2-} \rightarrow H_2O + 2e^- \tag{6}$$

$$\text{Cathode}: \quad O_2 + 4e^- \rightarrow 2O^{2-} \tag{7}$$

Generally, cell voltage is a function of various parameters such as current density, temperature, pressure and the gas composition [66]. In an actual cell unit, the cell voltage is below the idea one because of voltage drop caused by overpotentials, i.e., activation polarization, Ohmic loss and concentration polarization [47]. In this study, a specific fuel cell stack is not taken into consideration but a simplified approach is selected. A reference cell voltage is assumed to be in a practical range and a correction from the cell operating pressure is used, as described in the following equation [30,34]:

$$V = V_{\text{ref}} + \Delta V = V_{\text{ref}} + (RT/4F)\ln\left(P/P_{\text{ref}}\right) \tag{8}$$

The reference value is adopted at a nominal design condition, i.e., 0.7 V at 800 °C and 3.5 bar [30]. Here, V_{ref} is the reference voltage, 0.7 V; R is the universal gas constant, 8.31 J K^{-1} mol; T is the cell operating temperature, K; F is the Faraday constant, 96 486 J V^{-1} mol; P is the cell operating pressure, bar and P_{ref} is a reference pressure, 3.5 bar [30].

Table 2
Main design assumptions adopted in the simulation.

Air separation unit (ASU)	Oxygen purity, 95 vol% Oxygen pressure to gasifier, 40 bar Specific work, 0.325 kW h kg^{-1} O_2
Coal handing and milling	0.022 kW h kg^{-1} coal
Gasification process (Shell)	Gasification temperature, 1371 °C (slagging condition) Pressure, 32 bar Carbon conversion, 99.5% Oxygen/coal ratio (kg kg^{-1}), 0.9 CO_2/coal ratio (kg kg^{-1}), 0.11 Pressure drop, 5% Heat loss, 0.5% of input LHV Coal feedstock, 1 kg s^{-1} Gas quench type Auxiliary power for gasification, 0.5% of input LHV
Syngas quench and conditioning	Syngas temperature after quench, 900 °C Temperature of the quench gas, 350 °C Quench gas ratio, 49.1% Quench gas compressor efficiency, 75%
Convective heat exchangers in the waste boiler	Pressure drop, 2% Approach point ΔT, 10 °C
Gas cleaning	Pressure drop for fly ash removal, 6% Desulfurization, MEDA method Sulfur removal yield, 98% Desulfurization pressure drop, 6%
Chemical looping hydrogen generation process	Oxygen carrier: fuel reactor outlet, $Fe_{0.947}O/Fe_3O_4$; steam reactor outlet, Fe_3O_4; air reactor, Fe_2O_3; inert support, $FeAl_2O_4$ $Fe_2O_3/FeAl_2O_4$ (kg kg^{-1}), 1/1 Fuel reactor temperature, 950 °C upper riser, 800 °C bubbling bed. Steam reactor temperature, 750–800 °C Air reactor temperature, 950 °C Pressure drop, 8% Heat loss, 0.5% of thermal input
Solid oxide fuel cell	Operating temperature, 800–1000 °C Operating pressure, 2.5–20 bar Fuel utilization factor: 0.75–0.90 DC–AC inverter efficiency, 95%
Gas turbine cycle	Discharge pressure, 1.1 bar Turbine polytropic efficiency, 90% Mechanical/generator efficiency, 99%/99%
Heat recovery steam generation	Approach point ΔT, 10 °C Pinch point, 8 °C Pressure drop, 10% Thermal loss, 1% of thermal input
Steam turbine cycle (Rankine)	Pressure levels, 12.5/2.86/0.4 MPa IP steam reheat Condenser pressure, 3.6 kPa Steam turbine polytropic efficiency, HPST 89%, IPST 92%, LPST 85%
CO_2 compression	Single-stage compression ratio, 3.5 Compressor efficiency, 75% Cooling water temperature, 15 °C Mechanical/electrical efficiency, 99%/99% CO_2 for pipeline, 30 °C and 120 bar

The direct current (DC) power output from the SOFC stack is calculated as following:

$$W_{\text{SOFC·DC}} = VI = Vn_{H_2} \cdot 2F \tag{9}$$

To meet the grid requirement, the DC power from SOFC must be converted to AC, and filtered from possible oscillations for power distribution [28]. The efficiency of DC-AC inverter is assumed $\eta_{\text{inverter}} = 95\%$, and the actual AC power production is given by:

$$W_{SOFC\cdot AC} = \eta_{inverter} W_{SOFC\cdot DC} \quad (10)$$

The fuel cell is simulated with a lumped volume model. It calculates SOFC energy balance, thermodynamic properties and chemical compositions of anode and cathode outlet and stack exhaust gases, as a function of reactant utilization factors and inlet compositions.

2.4. Gas turbine cycle

The gas turbine cycle includes an air compressor, a combustor, a gas turbine and a CO_2 expander. The air compressor and the gas turbine could be connected in a single shaft. Air from the air compressor enters the air reactor, and then goes to the cell cathode. The cathode exhausted air and unconverted hydrogen from the anode burn in the combustor. The high pressure and high temperature exhaust gas from the combustor is supplied to the gas turbine. The high temperature CO_2-rich stream from the fuel reactor is also led to a CO_2 expander for additional electricity generation.

2.5. Steam turbine cycle

The steam turbine cycle is mainly comprised of a steam turbine, an air HRSG and a CO_2 HRSG. The waste boiler in the gasification block is also incorporated with the two HRSGs for steam raising. Heat exchangers in HRSGs and the waster boiler are ranged in series of economizers, evaporators, superheaters and reheaters, which means the plant system is in a high level of heat integration of HRSG and other process units. The high pressure (HP) live steam is 12.5 MPa/565 °C, the reheating steam is 2.86 MPa/565 °C, and the low pressure (LP) steam is 0.4 MPa/286 °C. After the expansion of HP steam, the outlet stream from the high pressure steam turbine (HPST) is subdivided into two parts: one is injected to the steam reactor for hydrogen generation, and the other is led to the reheater. The reheating steam enters the intermediate pressure steam turbine (IPST) and further expands in the low pressure steam turbine (LPST). An important parameter defining the HRSG performance is the pinch point and approach point [28]. The pinch point is 8 °C, and the approach point is 10 °C. The back pressure of condenser is 3.6 kPa. The polytropic efficiency of HPST, IPST, and LPST is 88%, 92% and 85%, respectively.

2.6. CO_2 separation and compression

After cooling in the CO_2 HRSG to 70 °C, the CO_2-rich stream primarily consists of steam vapor (a little water) and CO_2. Steam is condensed and removed in a condenser. The resulting CO_2 stream is then compressed in four stages and cooled using environmental water in each stage, removing residual water. Finally, CO_2 is compressed to 120 bar and ready for pipeline.

3. Plant performance evaluation

The power efficiency of the hybrid plant is defined below:

$$\eta_e = \frac{W_{net}}{m_{coal}\cdot LHV_{coal}} \quad (11)$$

η_e – plant power efficiency, %, which is also called electrical efficiency;
W_{net} – net power of the hybrid plant, kW;
m_{coal} – coal mass flow, kg s^{-1};
LHV_{coal} – coal lower heating value, kJ kg^{-1}.

The plant net power is calculated according to:

$$W_{net} = W_{SOFC\cdot AC} + W_{GT} + W_{ST} + W_{CO_2\cdot EX} - W_{ASU} - W_{CO_2\cdot C} - W_{COAL\cdot PRE} - W_{AUX} \quad (12)$$

Where W indicates power generation or consumption by each component, kW;

$W_{SOFC\cdot AC}$ – SOFC power, kW;
W_{GT} – gas turbine power, kW;
W_{ST} – steam turbine power, kW;
$W_{CO_2\cdot EX}$ – CO_2 expander power, kW;
W_{ASU} – ASU power, kW;
$W_{CO_2\cdot C}$ – CO_2 compression power, kW;
$W_{COAL\cdot PRE}$ – coal preparation power, kW;
W_{AUX} – auxiliary power, includes blowers, pumps and other devices, kW.

4. Plant performance

The primary assumptions are summarized in Table 2. The simulation result shown in Table 3 is a base case. As a whole, the CLHG-SOFC/GT power plant is more efficient than traditional pulverized coal plants and IGCC, even without CO_2 capture. The CLHG-SOFC/GT plant with CCS could achieve around 43.5% (LHV) efficiency. The advanced ultra-supercritical PC plant is around 41.7% (LHV) and IGCC is 40.8% (LHV) [67], when CCS is implemented, these efficiencies would be further reduced by 8–12 percentages.

In addition to the power efficiency advantages, the proposed CLHG-SOFC/GT plant has significant environmental benefits as well. The plant has low pollutants emissions, and 100% of the CO_2 is captured and sequestered for pipeline. Moreover, the fuel into the cell is hydrogen, and the risk of carbon deposition on the anodic electrodes is also avoided.

5. Sensitivity analysis

Sensitivity analysis could offer a deeper understanding over the entire plant. Some of the parameters in a hybrid system are flexible, while others cannot be changed freely. For example, the operating condition of gasifier is associated with the detailed design that is provided by gasifier vendors. The optimization of the gasifier and other component such as heat exchangers is beyond the scope of this work. General strategies that may decide the plant performance, such as system pressure, cell temperature, fuel utilization factor, CO_2 expander exhaust pressure and gas preheating modification are discussed in the following sections.

Table 3
Power balance and plant performance, SOFC operating temperature 900 °C, system pressure 20 bar, fuel utilization factor 0.75 and the steam reactor temperature 800 °C.

Coal LHV input, kW	26 805 (1 kg s^{-1})
Coal handling power, kW	79.20
ASU power, kW	1053
Syngas recycling, kW	54.06
SOFC, kW	3666.31
Gas turbine, kW	4449.67
Steam turbine, kW	4135.34
CO_2 expander, kW	1658.68
CO_2 compressors, kW	921.14
BOP, kW	134.38
Plant electrical efficiency, %	43.53
CO_2 capture efficiency, %	100

5.1. System operating pressure and cell temperature

The influences of system operating pressure and cell temperature on the plant performance are shown in Fig. 3a. In this example, the system operating pressure or cell temperature is varied while keeping other parameters constant. The fuel utilization factor U_f is 0.75. The operating pressure is varied in the range of 2.5 and 20 bar with a 2.5 bar increment, and the temperature span is between 800 °C and 1000 °C with a 100 °C increment. A value beyond 1000 °C is not adopted because it would exceed the operating range of the cell. As expected, with the increase of system pressure, the plant power efficiency increases, but with a diminishing return. Higher cell temperature also allows higher plant power efficiency, but its effect is not much significant as the effect of operating pressure. Fig. 3b shows the specific work outputs and inputs by different devices with the variation of system pressure at cell temperature 900 °C. With the rise of system pressure, the cell power output increases slightly. This is because the higher reactant partial pressure enhances electrochemical kinetics and the cell voltage increases according to Eq. (8). The power of gas turbine has a significant boost due to a higher pressure ratio. Although the air compressor consumes more power when the pressure ratio increases, the increase of the power generated by the turbine is more than the increased compressor power demand. Steam raising in HRSG is associated with the exhaust temperature of gas turbine upstream. As the system pressure increases, the exhaust temperature of gas turbine is reduced sharply. At an operating pressure of 2.5 bar, the exhaust temperature of gas turbine is 1105 °C, while it drops to 536 °C at a pressure of 20 bar. This directly results in a drop of steam generation from HRSG and the power of steam turbine decreases. The power of CO_2 expander increases with a rise of pressure because of a constant CO_2 expander exhaust pressure.

Taking the example of 900 °C as the base case, Fig. 3c shows the specific work changes of different devices at 800 °C and 1000 °C. It is seen that the SOFC power, the gas turbine power and the steam turbine power all increases with the rise of cell operating temperature, and at higher operating pressure, the power increment gap is larger except for the steam turbine. According to the Eq. (8), the cell voltage value increases by raising the cell temperature, which enhances the power output of SOFC. The gas turbine inlet and outlet temperatures increase at a higher cell temperature. At the pressure of 20 bar and cell temperature of 800 °C, the gas turbine inlet temperature is 1181 °C, while it increases to 1189 °C at a cell temperature of 1000 °C. Even though the temperature increment is less than 10 °C from 800 °C to 1000 °C, it leads to an increase in the power output from gas turbine and steam turbine. Higher cell temperature and especially higher operating pressure determine a remarkable enhancement of the electrical efficiency of the plant. However, the capital cost of the cell is usually a temperature-dependent function [47]: higher materials costs for cells and turbines must be taken into consideration when the value levels of the cell temperature and system pressure are increased.

5.2. Fuel utilization factor

The fuel utilization factor U_f is one of the key parameters in cell stack design. Fuel utilization factor is defined as the amount of fuel

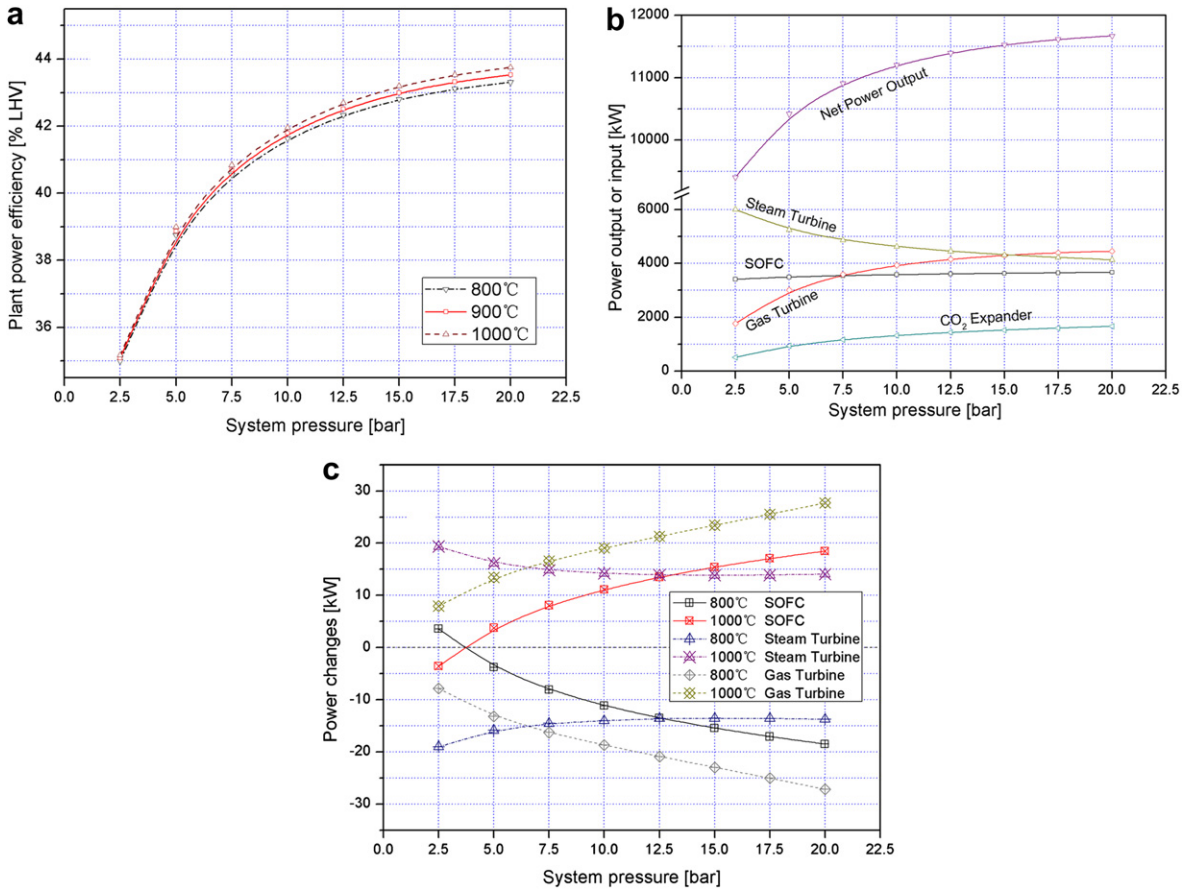

Fig. 3. Plant performance versus system operating pressure and cell temperature (a) plant power efficiency; (b) specific work of different devices with the variation of system pressure at cell temperature 900 °C; (c) specific work changes of different devices at 800 °C and 1000 °C.

reacted in the cell divided by the total inlet fuel. In this study, the fuel utilization factor is varied from 0.75 to 0.90 with a 0.05 increment. Values above 0.90 are not applicable because it is difficult for the cell to get such a high utilization factor limited by kinetics. Values below 0.75 are also not suitable because it may results in a temperature rising beyond the maximum allowable turbine inlet temperature. In this study, the other parameters are kept constant. The effects of fuel utilization on the plant electrical efficiency are shown in Fig. 4a. It is observed that with the increase of the fuel utilization factor, the plant electrical efficiency increases. Fig. 4b–d illustrates the specific work of the cell, gas turbine and steam turbine at varied fuel utilization factors and pressures. The fuel utilization factor has a significant impact on the specific work of the three devices, especially the cell. At a higher fuel utilization factor, the cell power has a sharp increase while there is a drop in the power output of gas turbine and the steam turbine. It is well known that fuel cells are expected to have a higher efficiency than gas turbines. At a higher fuel utilization factor more fuel is used in a more efficient way in the cells; on the contrary, lower fuel utilization factors lead to lower plant power efficiency because fuel is converted primarily in the combustor.

5.3. Steam reactor temperature

In CLHG system, the reactor temperature is an important parameter, especially the steam reactor. The temperature of each reactor must meet the following criteria: the first is heat balance, the heat required by the endothermic reaction in the reactors is provided by the sensible heat of solid oxygen carriers. The temperature of reactor must be kept at a constant value in normal operation through solid circulation without external heat addition; the second is the reactor temperature should be in an appropriate range for a better thermodynamics and kinetics. For the steam reactor, the reactions of metallic iron and wüstite with steam to magnetite are exothermic, and the hydrogen equilibrium is higher at a lower operating temperature. This means that at the same inlet flow rate of metallic iron and steam vapor, the hydrogen yield is larger at a lower temperature. However, the kinetics is poor at lower temperatures. Therefore, there is a compromise between thermodynamics and kinetics for steam reactor. The effects of steam reactor temperature on the plant power efficiency are shown in Fig. 5a. The fuel reactor temperature and the air reactor are held constant. The steam reactor temperature selected is from 750 °C to 800 °C with a 10 °C increment. Values below 750 °C are not included because of poor kinetics, and values above 800 °C are also infeasible because the steam reactor would require extra heat from outside, i.e., the heat integration is broken.

It is found that the steam reactor temperature has little impact on the plant power efficiency. Fig. 5b illustrates the variation of the specific work of each device involved in the plant. The power of the cell, CO_2 expander and CO_2 compressor remains little changed with the variation of the steam reactor temperature. As the rise of steam reactor temperature, the gas turbine power increases and the steam turbine power decreases. The increase of gas turbine power and the decrease of steam turbine power counteract each other and the gross power output of the plant is almost the same. The interpretation of this phenomenon is as follows: the cell power keeps unchanged because its operating temperature and pressure are held constant. At a lower steam reactor temperature, the solid oxygen carrier from the steam reactor to the air reactor has lower sensible heat. In order to guarantee the air reactor temperature at a constant level and a full oxidization of magnetite, the air flow into

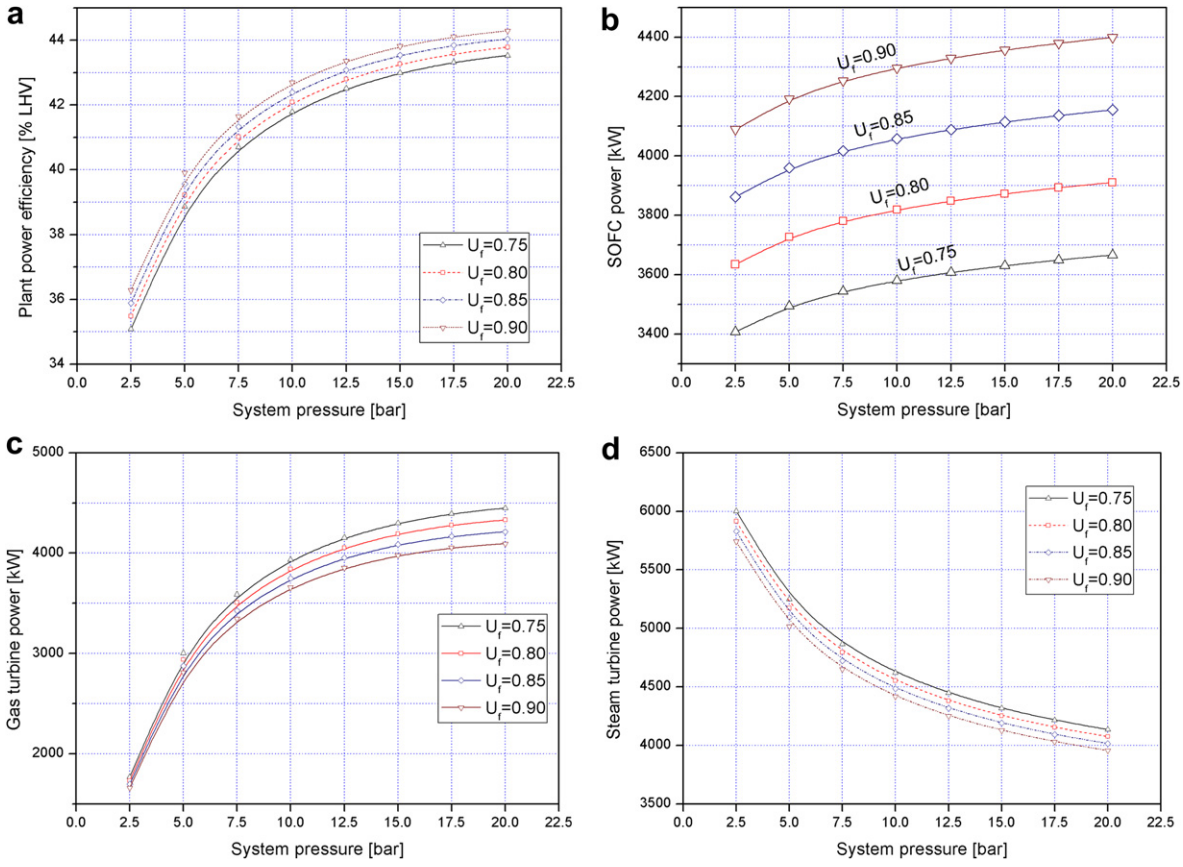

Fig. 4. Plant performance versus fuel utilization factor (a) plant power efficiency; (b) SOFC power; (c) gas turbine power; (d) steam turbine power.

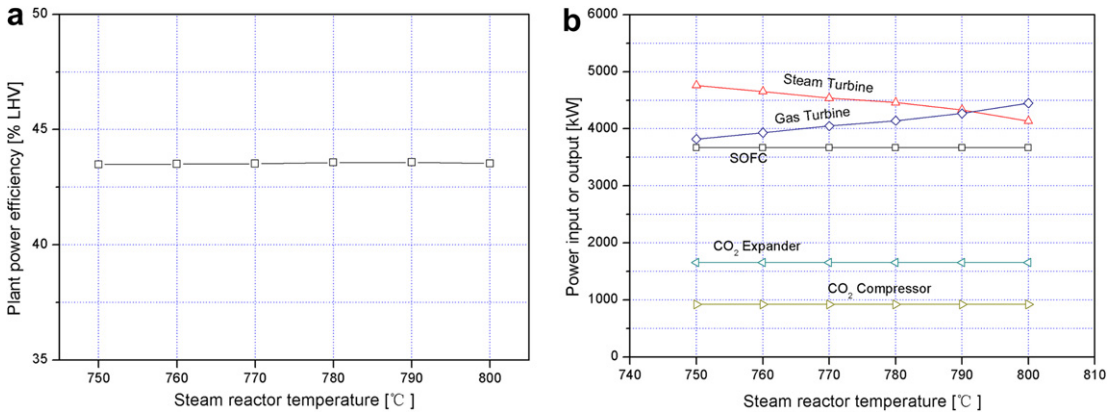

Fig. 5. Plant performance versus steam reactor temperature (a) plant power efficiency; (b) specific work of different devices.

the air reactor is reduced. The air stream is then led to the cell and the combustor. With a lower air flow, the combustion temperature increases and gives a higher turbine inlet temperature (TIT). At a steam reactor temperature of 750 °C, the TIT is 1235 °C while it drops to 1185 °C with a steam reactor temperature of 800 °C. However, the mass flow of gas turbine increases with the rise of steam reactor temperature. At 750 °C, the mass flow of gas turbine is 35 080 kg h^{-1} and it increases to 42 255 kg h^{-1} at 800 °C. Even though the TIT temperature increases, the total mass flow through the gas turbine decreases. The power output of the gas turbine increases at a larger mass flow with the same pressure ratio. Thus the gas turbine power output is smaller at a lower steam reactor temperature.

As to steam turbine, its power output decreases with the rise of steam reactor temperature. At a lower steam reactor temperature, the temperature of the exhaust stream from the gas turbine is higher, and the steam generation is larger. At a steam reactor temperature of 750 °C, the steam generation is 14 291 kg h^{-1} and at 800 °C it is 13 895 kg h^{-1}. At a higher steam reactor temperature, the hydrogen equilibrium is lower. In order to get a full conversion of wüstite to magnetite, more steam is injected into the steam reactor. The steam is bled from the steam turbine. At 750 °C, the steam bled is 4762 kg h^{-1} and increases to 6085 kg h^{-1} at 800 °C. This directly results in a decline in the power output of steam turbine. The effects of gas turbine and steam turbine offset each other and the power efficiency is kept almost the same. But from the point of view of kinetics, a higher steam reactor temperature is more favorable.

5.4. CO_2 expander exhaust pressure

As a benefit of CLHG system, CO_2 is inherently separated from the flue gas stream, and no additional CO_2 removal process is needed. After CO_2 expander and CO_2 HRSG, CO_2 is required to be compressed to a liquid state for pipeline and storage. The exhaust pressure of CO_2 expander is a parameter which influences the plant power efficiency in a certain degree. A lower expander exhaust pressure gives a higher CO_2 expander power, but the power consumption by the compressors is increased, and vice versa. Thus there is a compromise between the CO_2 expander and CO_2 compressors.

In the base case, the CO_2 expander exhaust pressure is set to 1.2 bar. Fig. 6a shows the plant power efficiency increment with the variation of CO_2 expander exhaust pressure. The system operating pressure is between 5 and 20 bar. With the increase of CO_2 expander exhaust pressure; there is an augment in plant power efficiency. Higher system operating pressure gives a higher efficiency increment. The efficiency enhancement declines as the exhaust pressure exceeds an optimum value. Fig. 6b illustrates the changes of the specific work of each device under varied system pressure, including steam turbine, CO_2 compressors and CO_2 expander. Obviously, the CO_2 compression work is reduced. It is observed that the steam turbine power increases with rise of the CO_2 expander exhaust pressure. This is because the temperature of CO_2 stream at the outlet of CO_2 expander increases at a higher exhaust pressure, which enhances the steam raising in the later CO_2 HRSG.

5.5. Inlet gas preheating

In most of the hybrid solid oxide fuel cell-gas turbine system, natural gas is usually used as fuel [28,44,45,53]. Natural gas must be preheated and reformed to CO and H_2 before electrochemical reaction in the cell stack. The preheating for air into the cell stack is also essential because large temperature differences between the inlet gas stream and cell stack may cause thermal stress [33]. The reforming of natural gas could be in an individual reformer, i.e., external reforming. The natural gas could also be reformed in the anode, i.e., internal reforming. The inlet gas stream including air and fuel needs to be preheated. There are usually two configurations for gas preheating [50]. One is using heat exchangers. The inlet gas is heated by the exhaust gas from the cell or combustor. The other is gas recirculation. The high-temperature flue gas from the cell or combustor is recycled and mixed with the inlet gas, i.e., the internal reheating. This removes the need for a heat exchanger, and the gas recirculation could be driven by a fresh-gas-driven jet ejector [40,53], which eliminates the high-temperature blower. Air recycling will has a negative effect on cell performance by reducing the oxygen concentration in the cathode [53]. But fuel stream recycling is usually adopted in natural gas hybrid solid oxide fuel cell-gas turbine system since it offers higher plant efficiency [36,38,53,68]. In CLHG, the air into the cathode is from the air reactor, and the hydrogen into the anode comes from the steam reactor. The inlet gas streams to the cell are at a lower or higher temperature in the base case of cell temperature 900 °C. The inlet hydrogen is at 800 °C, the inlet air is at 950 °C and the cell is at 900 °C. Even though the maximum temperature discrepancy is 150 °C, which is below the upper limit of 200 °C [30,31], it is an alternative way to further reduce the temperature discrepancy to alleviate the stack thermal stress for a longer cell lifetime. Four modifications are presented to preheat inlet hydrogen to 900 °C, as follows:

(i) Case 1: preheating hydrogen using inlet air through heat exchangers;

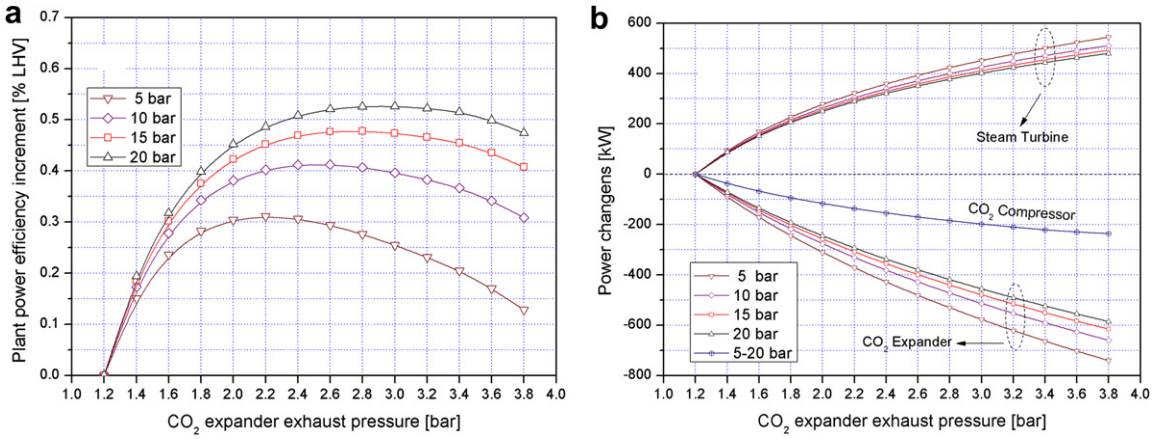

Fig. 6. Plant performance versus CO_2 expander exhaust pressure (a) plant power efficiency increment; (b) specific work changes of different devices.

Table 4
A summary of power and efficiency in cases.

	Case 1	Case 2	Case 3	Case 4	Base case
Power units					
SOFC, kW	3666.31	3666.31	3666.31	3666.31	3666.31
Gas turbine, kW	4449.67	4437.98	4437.99	4424.96	4449.67
Steam turbine, kW	4135.34	4129.42	4192.41	4122.77	4135.34
CO_2 expander, kW	1658.68	1658.68	1658.68	1658.68	1658.68
Plant electrical efficiency, %	43.53	43.47	43.47	43.39	43.53

(ii) Case 2: preheating hydrogen using anode exhaust through heat exchangers;
(iii) Case 3: preheating hydrogen using air reactor exhaust through heat exchangers;
(iv) Case 4: preheating hydrogen through recycling a fraction of anode exhaust.

Table 4 shows a comparison of the specific power and plant power efficiency. Interestingly, there are some changes in the power output of components, but the net plant efficiency is nearly kept the same. This means that these modifications are applicable without plant efficiency defect. Compared with the natural gas hybrid system, the preheating mode of inlet fuel gas in CLHG-SOFC/GT has little impact on the system performance. In CLHG-SOFC/GT, the inlet fuel gas into the cell is hydrogen, and the reforming process is eliminated. Reforming is a strong endothermic reaction. The factors related to reforming such as steam/carbon ratio, temperature and reforming modes (external or internal) directly influence the global heat integration and further determine the plant power efficiency. Therefore, the natural gas hybrid system performance is very sensitive to the preheating configuration and reforming modes. In CLHG-SOFC/GT, the inlet gas stream is already at a temperature close to the cell operating temperature. The preheating modification above plays a minor role in system efficiency, but they are helpful in the aspect of stack mechanical thermal stress. A large temperature difference at the cell will cause mechanical problems mainly due to excessive thermal stress evolution inside the cell.

6. Conclusions

This study integrated an SOFC/GT hybrid cycle with coal gasification and CLHG for power generation. CO_2 is inherently separated within the plant system. The hybrid system has a high electrical efficiency and an excellent environmental performance. The plant could achieve an electrical efficiency above 43.5% with 100% CO_2 capture. The following are some of the inferences from the current work.

Higher system pressure gives higher plant power efficiency, and higher cell temperature also increases the plant power efficiency, because the cell voltage increases as operating pressure and temperature increases. But the effect of temperature is not much significant as the effect of pressure. Fuel utilization factor is an important parameter in the system. It allocates the power distribution in each component. Higher cell fuel utilization factor allows higher plant power efficiency because the efficiency of the SOFC is higher than gas turbine. With the increase of CO_2 expander pressure, the CO_2 compressor power is decreased. There is a compromise between CO_2 expander and CO_2 compressors. The optimal CO_2 expander pressure depends on system pressure. Steam reactor temperature has littler effects on the system efficiency, but a higher steam reactor temperature is preferred because of a better kinetics in the steam-iron process. Gas preheating is an approach to alleviate temperature differences inside the cell, the implementation of gas preheating has almost no impact on the plant power efficiency.

Acknowledgments

The authors wish to express thanks to the National Natural Science Foundation of China (51176033), the Foundation of Graduate Creative Program of Jiangsu (CXZZ-0147) and the Scholarship Award for Excellent Doctoral Student Granted by Ministry of Education for financial support of this project.

References

[1] IPCC report. Special Report on Renewable Energy Sources and Climate Change Mitigation. Available from: http://srren.ipcc-wg3.de/.
[2] T. Nakata, D. Silva, M. Rodionov, Prog. Energy Combust. Sci. 37 (2011) 462–502.
[3] DOE report. Cost and Performance Baseline for Fossil Energy Plants. Volume 1: Bituminous Coal and Natural Gas to Electricity, National Energy Technology Laboratory, DOE/NETL 2010/197.
[4] M.M. Hossain, H.I. de Lasa, Chem. Eng. Sci. 63 (2008) 4433–4451.
[5] C. Linderholm, T. Mattisson, A. Lyngfelt, Fuel 88 (2009) 2083–2096.
[6] L.S. Fan, F. Li, Ind. Eng. Chem. Res. 49 (2010) 10200–10211.
[7] T. Mattisson, A. Lyngfelt, P. Cho, Fuel 80 (2001) 1953–1962.
[8] A. Abad, T. Mattisson, A. Lyngfelt, M. Johansson, Fuel 86 (2007) 1021–1035.
[9] P. Gayán, C. Dueso, A. Abad, J. Adanez, L.F. de Diego, F. García-Labiano, Fuel 88 (2009) 1016–1023.
[10] E. Jerndal, T. Mattisson, I. Thijs, F. Snijkers, A. Lyngfelt, Int. J. Greenhouse Gas Control 4 (2010) 23–35.
[11] S.Y. Chuang, J.S. Dennis, A.N. Hayhurst, S.A. Scott, Chem. Eng. Res. Des. 89 (2011) 1511–1523.

[12] S.Y. Chuang, J.S. Dennis, A.N. Hayhurst, S.A. Scott, Energy Fuels 24 (2010) 3917–3927.
[13] M. Ortiz, P. Gayán, L.F. de Diego, F. García-Labiano, A. Abad, J. Power Sources 196 (2011) 4370–4381.
[14] A.M. Kierzkowska, C.D. Bohn, S.A. Scott, J.P. Cleeton, J.S. Dennis, C.R. Müller, Ind. Eng. Chem. Res. 49 (2010) 5383–5391.
[15] V. Hacker, J. Power Sources 118 (2003) 311–314.
[16] S.D. Fraser, M. Monsberger, V. Hacker, J. Power Sources 161 (2006) 420–431.
[17] C.D. Bohn, C.R. Müller, J.P. Cleeton, A.N. Hayburst, J.F. Davidson, S.A. Scott, et al., Ind. Eng. Chem. Res. 47 (2008) 7623–7630.
[18] C.R. Müller, C.D. Bohn, Q. Song, S.A. Scott, J.S. Dennis, Chem. Eng. J. 166 (2011) 1052–1060.
[19] S.Y. Chen, Q.L. Shi, Z.P. Xue, X.Y. Sun, W.G. Xiang, Int. J. Hydrogen Energy 36 (2011) 8915–8926.
[20] P. Gupta, L.G. Velazquez-Vargas, L.S. Fan, Energy Fuels 21 (2007) 2900–2908.
[21] C.D. Bohn, J.P. Cleeton, C.R. Müller, J.F. Davidson, A.N. Hayhurst, S.A. Scott, et al., AIChE J. 56 (2009) 1016–1029.
[22] K.S. Kang, C.H. Kim, K.K. Bae, W.C. Cho, S.H. Kim, C.S. Park, Int. J. Hydrogen Energy 35 (2010) 12246–12254.
[23] F. Li, H.R. Kim, D. Sridhar, F. Wang, L. Zeng, J. Chen, et al., Energy Fuels 23 (2009) 4182–4189.
[24] K. Svoboda, G. Slowinski, J. Rogut, D. Baxter, Energy Convers. Manage. 48 (2007) 3063–3073.
[25] A. Messerschmitt, Process of Producing Hydrogen, U.S. Patent 465,686, 1910.
[26] V. Hacker, R. Fankhauser, G. Faleschini, H. Fuchs, K. Friedrich, M. Muhr, et al., J. Power Sources 86 (2000) 531–535.
[27] J.B. Yang, N.S. Cai, Z.S. Li, Energy Fuels 22 (2008) 2570–2579.
[28] A. Arsalis, J. Power Sources 181 (2008) 313–326.
[29] P. Dokmaingam, J.T.S. Irvine, S. Assabumrungrat, S. Charojrochkul, N. Laosiripojana, Int. J. Hydrogen Energy 35 (2010) 13271–13279.
[30] S.K. Park, T.S. Kim, J. Power Sources 163 (2006) 490–499.
[31] W.J. Yang, S.K. Park, T.S. Kim, J.H. Kim, J.L. Sohn, S.T. Ro, J. Power Sources 160 (2006) 462–473.
[32] S.K. Park, J.H. Ahn, T.S. Kim, Appl. Energy 88 (2011) 2976–2987.
[33] S.K. Park, K.S. Oh, T.S. Kim, J. Power Sources 170 (2007) 130–139.
[34] S.K. Park, T.S. Kim, J.L. Sohn, Y.D. Lee, Appl. Energy 88 (2011) 1187–1196.
[35] Y. Yi, A.D. Rao, J. Brouwer, G.S. Samuelsen, J. Power Sources 132 (2004) 77–85.
[36] M. Granovskii, I. Dincer, M. Rosen, J. Power Sources 165 (2007) 307–314.
[37] J. Palsson, A. Selimovic, L. Sjunnesson, J. Power Sources 86 (2000) 442–448.
[38] H. Uechi, S. Kimijima, N. Kasagi, J. Eng, Gas Turbines Power 126 (2004) 755–762.
[39] S. Campanari, ASME Paper No. GT2004–53933.
[40] S. Campanari, J. Power Sources 112 (2002) 273–289.
[41] A. Franzoni, L. Magistri, A. Traverso, A.F. Massardo, Energy 33 (2008) 311–320.
[42] T.H. Lim, R.H. Song, D.R. Shin, J.I. Yang, H. Jung, I.C. Vinke, et al., Int. J. Hydrogen Energy 33 (2008) 1076–1083.
[43] B.F. Möller, J. Arriagada, M. Assadi, I. Potts, J. Power Sources 131 (2004) 320–326.
[44] T.A. Adams II, P.I. Barton, J. Power Sources 195 (2010) 1971–1983.
[45] T. Kuramochi, W. Turkenburg, A. Faaij, Fuel 90 (2011) 958–973.
[46] Y. Haseli, I. Dincer, G.F. Naterer, Int. J. Hydrogen Energy 33 (2008) 5811–5822.
[47] F. Calise, M.D. d'Accadia, A. Palombo, L. Vanoli, Energy 31 (2006) 3278–3299.
[48] World Coal Institute. Available from: http://www.worldcoal.org/.
[49] S. Ghosh, S. De, Energy 31 (2006) 345–363.
[50] M.C. Williams, J. Strakey, W. Sudoval, J. Power Sources 159 (2006) 1241–1247.
[51] T. Kivisaari, P. Björnbom, C. Sylwan, B. Jacquinot, D. Jansen, A. de Groot, Chem. Eng. J. 100 (2004) 167–180.
[52] K.D. Panopoulos, L.E. Fryda, J. Karl, S. Poulou, E. Kakaras, J. Power Sources 159 (2006) 570–585.
[53] E. Liese, J. Eng. Gas Turbines Power 132 (2010) 061703.
[54] T.A. Adams II, P.I. Barton, AIChE J. 56 (2010) 3120–3136.
[55] M.A. Khaleel, Z. Lin, P. Singh, W. Surdoval, D. Collin, J. Power Sources 130 (2004) 136–148.
[56] D. Bhattacharyya, R. Turton, S.E. Zitney, Ind. Eng. Chem. Res. 50 (2011) 1674–1690.
[57] W.G. Xiang, S.Y. Chen, Z.P. Xue, X.Y. Sun, Int. J. Hydrogen Energy 35 (2010) 8580–8591.
[58] J.P.E. Cleeton, C.D. Bohn, C.R. Müller, J.S. Dennis, S.A. Scott, Int. J. Hydrogen Energy 34 (2009) 1–12.
[59] C. Cormos, Int. J. Hydrogen Energy 36 (2011) 5960–5971.
[60] C. Cormos, Int. J. Hydrogen Energy 32 (2010) 2278–2289.
[61] P. Chiesa, G. Lozza, A. Malandrino, M. Romano, V. Piccolo, Int. J. Hydrogen Energy 33 (2008) 2233–2245.
[62] Y. Huang, S. Rezvani, D. McIlveen-Wright, A. Minchener, N. Hewitt, Fuel Process. Technol. 89 (2008) 916–925.
[63] J. Davison, Energy 32 (2007) 1163–1176.
[64] A. Giuffrida, M.C. Romano, G.G. Lozza, Appl. Energy 87 (2010) 3374–3383.
[65] J.A. Matelli, E. Bazzo, J. Power Sources 142 (2005) 160–168.
[66] M.C. Romano, S. Campanari, V. Spallina, G. Lozza, ASME Paper No. GT2009-59551.
[67] DOE report. Cost and Performance Baseline for Fossil Energy Plants. Volume 3a: Low Rank Coal to Electricity: IGCC Case, National Energy Technology Laboratory, DOE/NETL 2010/1399.
[68] L.Q. Duan, X. Wang, Y.P. Yang, B.B. He, ASME Paper No. GT2009-59497.